ORIGINAL ARTICLE

Study on arc behavior and droplet transfer in twin-electrode TIG-MIG indirect arc welding

Yanli Zhu[1] · Zeli Wang[1] · Runtao Liu[1] · Liming Liu[1]

Abstract

A twin-electrode TIG-MIG (T-TIG-MIG) indirect arc welding method was proposed in this paper. The arc behavior and droplet transfer process were preliminarily investigated; moreover, the process stability was assessed, and bead-on-plate welding was conducted. Results showed T-TIG-MIG indirect arc burnt between a wire and two tungsten electrodes and was essentially formed by the coupling of two single-electrode TIG-MIG indirect arcs. The wire feeding speed (WFS) determined the equilibrium position of the wire end, and the vicinity of the tungsten tips was an ideal position for arc shape and droplet detachment, where the arc was more concentrated with a higher coupling degree. With the increase of the welding current, the arc length and stiffness increased gradually; so did the process stability and the spreadability of the weld bead. When the current exceeded the critical current, the droplet transfer mode changed into streaming spray transfer, since the electromagnetic force and the arc pressure increased considerably. Compared to conventional cold-wire T-TIG welding under the same current, the wire deposition rate of T-TIG-MIG indirect arc welding increased by about 186%, while the range of the heat-affected zone reduced by about 41%.

1 Introduction

Tungsten inert gas (TIG) welding was an extensively applied joining process in the manufacturing industry due to its advantages of high arc stability, less spatter, outstanding weld quality, and easy automation [1, 2]. In order to achieve desirable welds, filler metals were generally required during the TIG welding process. Presently, there were two commonly applied methods for filling the joint: the cold-wire TIG welding process and hot-wire TIG welding process. In the cold-wire TIG welding process [3], the filler metal was directly added. To increase the melting speed of the wire, the filler metal was preheated by the resistive heat, while it was fed into the weld pool in the hot-wire TIG welding process [4]. However, this method could only be adopted for filler metals with high resistance and also existed strong deflection phenomenon of the arc due to the magnetic field

generated by the current in the filler metal. To eliminate the above defects in hot-wire TIG welding process, a series of improved methods were successively developed. Lv et al. [5] established an assistant arc to preheat the wire for hot-wire welding process and asserted that the new method was suitable for low resistance wire such as copper and aluminum and further claimed that the deposition rate of the HS201 wire could be increased by 96% compared with the conventional TIG welding method. Voigt et al. [6] developed a wire preheating system applying electromagnetic induction to the hot-wire GTAW process and found that this method could eliminate the magnetic blow phenomenon that existed in conventional hot-wire preheating method and achieve a higher wire melting speed.

Unfortunately, the wire melting was still finished by the heat generated from the weld pool in the hot-wire TIG welding process. In other words, a larger weld pool was necessary to further increase the deposition rate of the wire. The arc energy and the wire deposition rate were thus coupled, which decreased the process controllability. Chen et al. [7] proposed an arcing-wire GTAW method, in which a side arc was established between the tungsten electrode and the filler metal inside the main TIG arc. The wire was almost

✉ Liming Liu
liulm@dlut.edu.cn

1 Key Laboratory of Liaoning Advanced Welding and Joining Technology, School of Materials Science and Engineering, Dalian University of Technology, Dalian 116024, China

completely melted by the side arc, not relying on the weld pool. In other words, arc energy and the wire deposition rate were decoupled. Wang et al. [8] developed a consumable and nonconsumable electrode indirect arc welding, in which the current flowed from the consumable electrode to the non-consumable electrode, while no current passed through the workpiece and found that it could not only considerably enhance the melting speed of the wire but also restrain the heat input to the workpiece.

Previously, a T-TIG welding method was proposed to improve the welding efficiency [9]. In this method, two insulated tungsten electrodes set at a small distance were connected to respective power sources, and then a coupling arc was produced by the interaction of two arcs generated from the two electrodes, respectively. Leng et al. [10, 11] proposed that the arc pressure of T-TIG was considerably lower than that of single-electrode TIG welding under similar heat input; consequently, T-TIG achieved to weld thick plate with a high deposition rate because of its stable weld pool under high current.

In this study, combining the characteristics of the indirect arc and T-TIG, the T-TIG-MIG indirect arc welding method was proposed. The arc behavior and droplet transfer process of T-TIG-MIG indirect arc welding were preliminarily investigated by experiments, and the physical models were constructed to reveal the mechanisms of the arc formation and droplet detachment.

2 Experimental methods

Figure 1 shows the T-TIG-MIG indirect arc welding system. It was mainly composed of two TIG welding torches, one MIG welding torch, two TIG power sources (OTC AEP-500), and one wire feeder. These welding torches were placed in a circular array by a self-designed fixture, and specifically, the wire was located in the symmetrical plane of the two tungsten electrodes. The two electrodes were connected to the cathodes of the two power sources, respectively, while the wire was connected to their anodes in common. However, the workpiece was not connected to the power sources. Q235 low carbon steel plates with a dimension of $200 \text{ mm} \times 150 \text{ mm} \times 7 \text{ mm}$ were employed as the workpiece for bead-on-plate welding, and ER50-6 low carbon steel wires with a diameter of 1.2 mm were selected as the filler metal. Their chemical compositions are listed in Table 1. The shielded gas was 99.99% highly pure argon gas. When welding, the welding torches remained stationary,
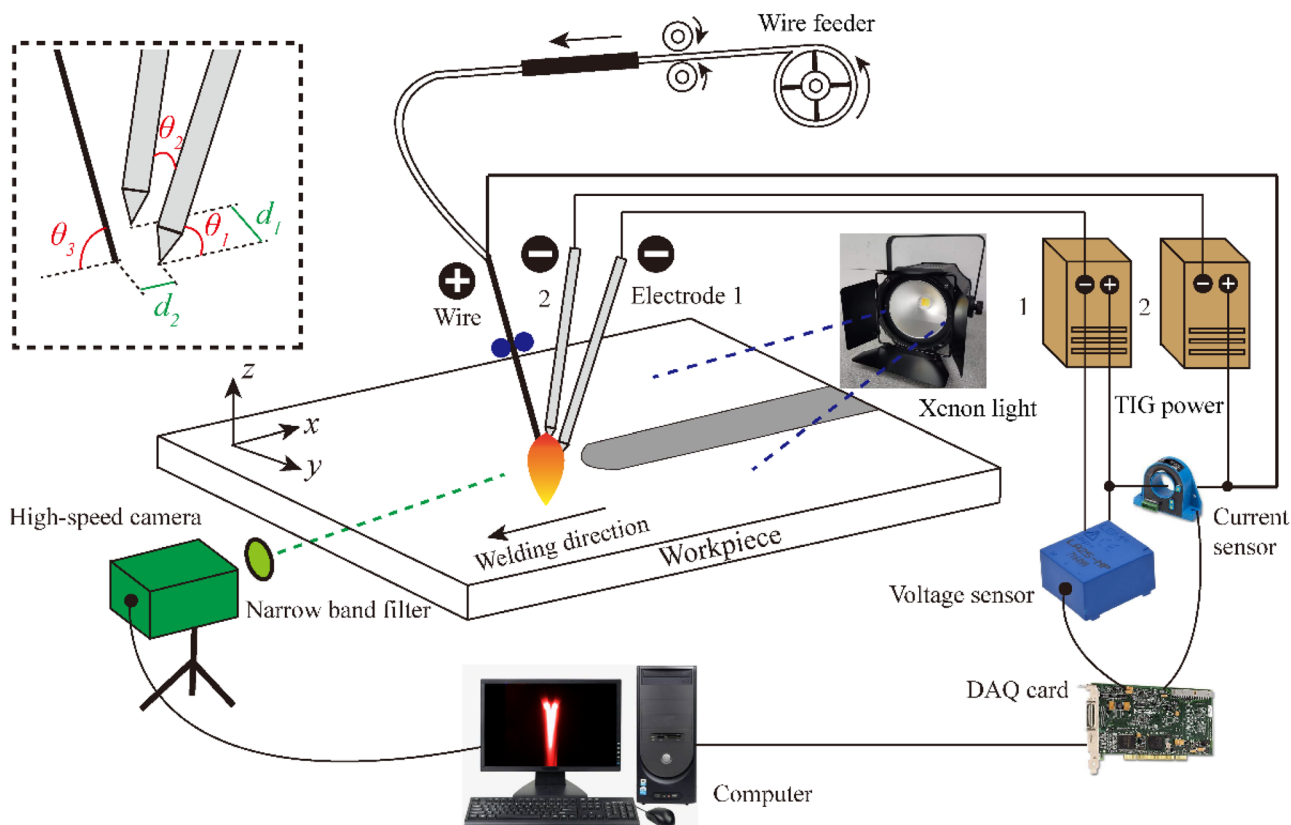

Fig. 1 Schematic diagram of T-TIG-MIG indirect arc welding system

Table 1 Chemical composition of the workpiece and the wire (wt. %)

	C	Mn	Si	S	P	Fe
Q235	0.15	0.50	0.20	0.03	0.03	Re
ER50-6	0.078	1.45	0.87	0.013	0.012	Re

while the workpiece moved. The detailed welding parameters are listed in Table 2. Two groups of experiments were conducted to study the influences of the WFS and welding current on the arc behavior and droplet transfer process, respectively. The specific experimental parameters are shown in Table 3, and other welding parameters are set as constants.

A high-speed camera was employed to acquire the arc shape and the droplet transfer process of T-TIG-MIG indirect arc welding. In this experiment, the settings of the high-speed camera were 320×240 pixel resolution, 500 μs exposure time, and 2000 fps acquiring frequency. A computer could display and save the arc image through corresponding software. In addition, to eliminate the interference of the arc light during capturing the droplet behavior, a xenon lamp was employed as the backlight and placed on the same line as the high-speed camera and the droplet. In order to monitor the stability of the T-TIG-MIG indirect arc welding process, the arc current and voltage signals were acquired by a current sensor and a voltage sensor, respectively, and then transferred to the A/D converter by a data acquisition (DAQ) card (NI PCI-6221). Consequently, the process stability could be evaluated by processing the acquired digital current and voltage signals according to statistical theories.

3 Results and discussions

3.1 Arc shape

The arc shape and the droplet transfer were consistent to some extent. The stable arc behavior would improve the smooth transfer of the droplet, and the stable transfer process of the droplet would keep the arc stable in turn. The WFS and welding current were the most important factors affecting arc shape and droplet transfer during indirect arc welding [12]. In this section, the effects of WFS and welding current on the arc shape were investigated, respectively.

Figure 2 shows the arc shapes of T-TIG-MIG indirect arc welding under different WFSs. It could be seen that different WFSs led to different equilibrium positions of the wire end and further different final arc shapes. In Fig. 2a, b, a′, b′, at the WFSs of 285 and 295 cm/min, the end of the wire was located at the upper left of the tungsten tips in the *xOz* plane, which caused the arc to shift to the wire side and showed a large degree of the arc deflection. Meanwhile, the distance between the wire end and the electrode tips was large; thus, this arc was obviously elongated and dispersed and presented a significant fluctuation of the arc length. As the WFS increased to 315 and 335 cm/min, in Fig. 2c, d, c′, d′, the end of the wire was located at the left of the tungsten tips in the *xOz* plane, and the arc had a significant contraction with a small cross section. Besides, this arc was almost vertical, and its stiffness was higher. When the WFS reached 355 and 375 cm/min as shown in Fig. 2e, f, e′, f′, the end of the wire was located at the lower left of the tungsten tips in the *xOz* plane, which made the arc shifted to the electrode side and expanded again. Moreover, the degree of the arc deflection further increased with the increase of the WFS.

The arc shapes of T-TIG-MIG indirect arc welding with different currents under the corresponding WFSs are shown in Fig. 3. When the current was small in Fig. 3a, b, a′, b′, the arc length and outline of the arc were small with low

Table 2 Welding parameters

Parameter	Value
Tungsten diameter (mm)	3.2
Wire extension (mm)	25
Electrode angle, θ_1 (°)	70
Angle between electrodes, θ_2 (°)	40
Wire angle, θ_3 (°)	70
Electrode/electrode distance, d_1 (mm)	2
Wire/electrode distance, d_2 (mm)	2
Gas flow (L/min)	12
Electrode tip height (mm)	8
Welding velocity (mm/s)	6

Table 3 Experimental parameters

Number	Welding current (A)	WFS (cm/min)
I-1	120 + 120	285
I-2	120 + 120	295
I-3	120 + 120	315
I-4	120 + 120	335
I-5	120 + 120	355
I-6	120 + 120	375
II-1	60 + 60	160
II-2	80 + 80	200
II-3	100 + 100	250
II-4	120 + 120	315
II-5	140 + 140	410
II-6	160 + 160	510

Fig. 2 Arc shapes of T-TIG-MIG indirect arc welding with a current of 120 A + 120 A under different WFSs: **a, a′** 285 cm/min; **b, b′** 295 cm/min; **c, c′** 315 cm/min; **d, d′** 335 cm/min; **e, e′** 355 cm/min; and **f, f′** 375 cm/min
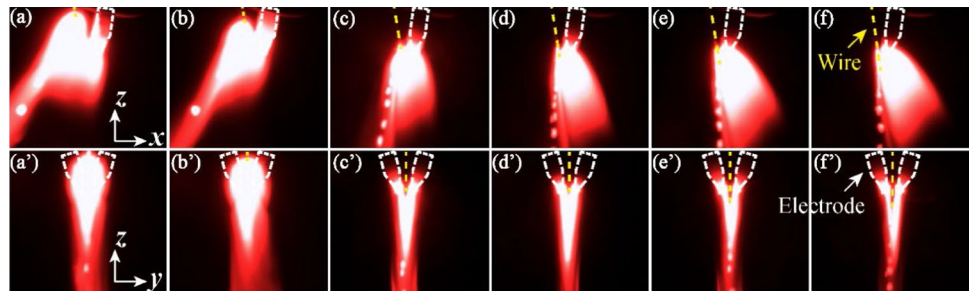
brightness and stiffness due to the low degree of gas ionization. Besides, the arc presented a significant fluctuation. In Fig. 3c–f, c′–f′, when the current was larger, the thermal power of the arc enhanced, and thus the degree of gas ionization remarkably increased, resulting in the arc length and brightness enlarging with a small amplitude of oscillation.

Since the workpiece was not connected to the power source, the arc was formed between a wire and two electrodes, where the current flowed from the wire to the two electrodes due to the potential difference, and then two closed current loops were produced. Figure 4 shows the magnetic field distribution generated by the currents in the wire and the electrodes. In the surrounded area between the wire and the electrodes, according to Ampere's law, the directions of the magnetic fields generated by the above two were the same, while outside this area, their magnetic field directions were opposite. Therefore, the total magnetic flux intensity in the upper arc column was greater than that in the lower arc column.

Ando and Hasegawa suggested that the charged particles in the arc plasma of conventional arc welding were mainly affected by electromagnetic force and plasma jet force [13]. In order to visually characterize the formation mechanism of the T-TIG-MIG indirect arc, two charged particles selected from the upper and the lower arc column, respectively, were subject to force analysis, as shown in Fig. 4.

When the WFS was suitable, the end of the wire was just near the tungsten tips in Fig. 4b, c. The charged particles in

the upper and lower arc columns were subjected to the electromagnetic forces F_{e1} and F_{e2}, respectively, while the directions of their components along the z-axis were opposite. Because the magnetic flux intensity in the upper arc column was larger, F_{e1} was greater than F_{e2} according to Ampere's law, and thus the component along the z-axis of the resultant electromagnetic force pointed downward. In other words, the electromagnetic force in the upper arc column played a more important role in determining the arc shape in this electrode arrangement. In addition, the components along the z-axis of the plasma jet forces F_{p1} and F_{p2} in the upper and lower arc columns both pointed downward. Therefore, the direction of the final arc shape pointed downward under the combined action of electromagnetic force and plasma jet force.

Different from the single-electrode TIG-MIG indirect arc, the T-TIG-MIG indirect arc essentially consisted of two indirect arcs that could affect each other. In Fig. 4c, the charged particles were also located in the magnetic field induced by the other arc, and thus subjected to the electromagnetic force F_d besides the two forces mentioned above. Apparently, the direction of the F_d pointed to the other arc. As a result, the two indirect arcs attracted each other and then coupled into an integrated arc.

However, when the WFS was relatively low in Fig. 4a, the directions of the electromagnetic force F_e and the plasma jet force F_p changed, and thus the resultant force pointed to the wire side, which resulted in a large degree of the arc deflection in xOz plane. In addition, owing to the increased
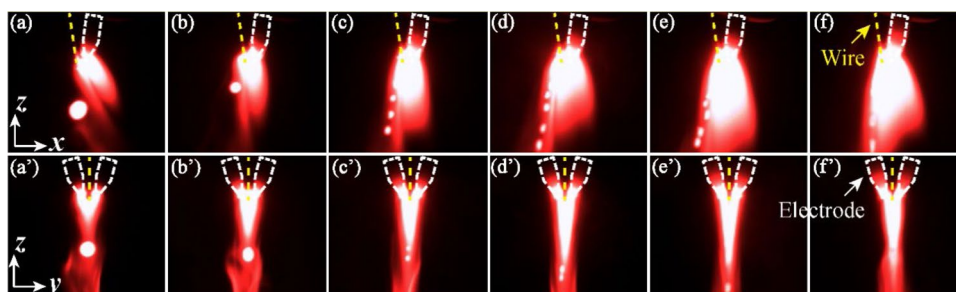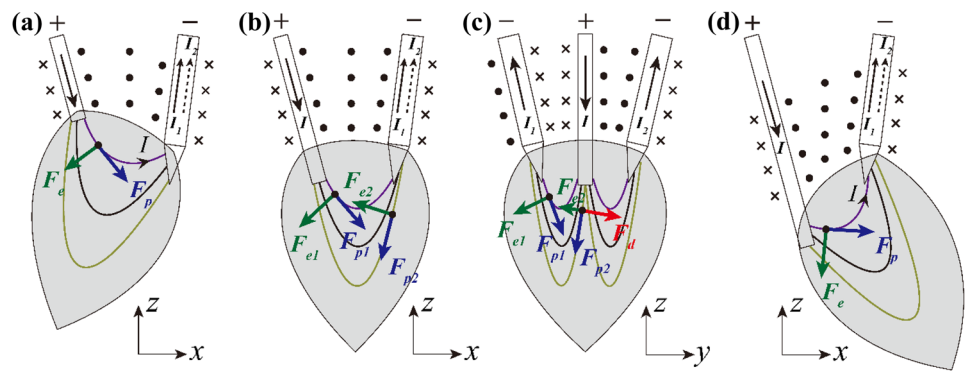

Fig. 3 Arc shapes of T-TIG-MIG indirect arc welding with different currents under the corresponding WFSs: **a, a′** 60 A + 60 A, 160 cm/min; **b, b′** 80 A + 80 A, 200 cm/min; **c, c′** 100 A + 100 A, 250 cm/min; **d, d′** 120 A + 120 A, 315 cm/min; **e, e′** 140 A + 140 A, 410 cm/min; and **f, f′** 160 A + 160 A, 510 cm/min

Fig. 4 Force analysis of charged particles in T-TIG-MIG indirect arc welding: **a** low WFS; **b**, **c** optimized WFS; and **d** high WFS

conductive channel, the arc current density and induced magnetic flux density decreased, and thus the electromagnetic force F_d was also reduced. Consequently, the coupling degree of the coupled arc decreased, which in turn made the arc more dispersed. Furthermore, when the WFS was relatively high in Fig. 4d, the resultant force of F_e and F_p also changed and pointed to the electrode side, and thus the coupled arc also deflected.

When the welding current was relatively small, the electromagnetic force F_e and the plasma jet force F_p were both low [14], which contributed to the low arc length and stiffness in Fig. 3a, b, a′, b′. However, as the current increased, especially exceeding the critical current, the degree of gas ionization and the arc current density increased substantially. Consequently, besides the F_e and F_p increasing considerably, the electromagnetic force F_d also enhanced significantly, which was helpful to achieve a coupled arc with a high arc length and stiffness in Fig. 3c–f, c′–f′.

3.2 Droplet transfer

In this section, the effects of WFS and welding current on the droplet transfer process were investigated respectively. Figures 5, 6, and 7 show the droplet transfer processes of T-TIG-MIG indirect arc welding with a current of 120 A + 120 A under different WFSs. Each image series showed a whole transfer period with different interval times. It could

be seen that different WFSs resulted in different relative positions between the wire end and the tungsten tips, and thus different thermal-force behavior of the droplet, which determined the droplet detachment.

As shown in Fig. 5, when the WFS was 295 cm/min, the droplet was detached from the wire at the upper left of the tungsten tips, and the droplet trajectory shifted to the wire side in the *xOz* plane. The diameter of the droplet was approximately equal to that of the wire, and the transfer frequency was about 117 Hz. The droplet transfer mode belonged to projected spray transfer [15]. Additionally, in the *yOz* plane in Fig. 5a′–f′, the droplet trajectory presented irregular, not located at the symmetry plane of the two tungsten electrodes, but deflected to one side.

When the WFS increased to 335 cm/min in Fig. 6, the melting speed of the wire increased, and the wire end had an obvious necking effect at the left of the tungsten tips in the *xOz* plane, and then a distinct fluid beam occurred hanging at the wire end. It was the primary characteristic of the streaming spray transfer. The diameter of the fluid beam was much smaller than that of the wire. Meanwhile, the droplet was formed at the bottom of the fluid beam, and smoothly detached from the bottom of the fluid beam. The droplet diameter decreased to about 0.79 mm, and the transfer frequency reached about 666.7 Hz. Besides, the droplet trajectory was nearly perpendicular and extremely regular.

When the WFS further increased to 375 cm/min, as shown in Fig. 7, the wire end also had the necking phenomena at the
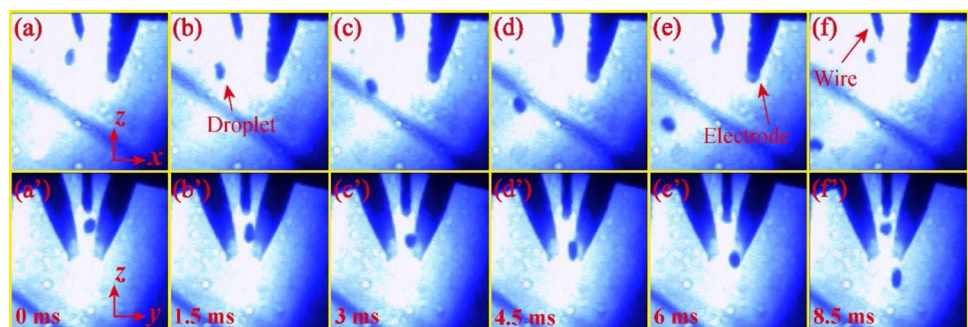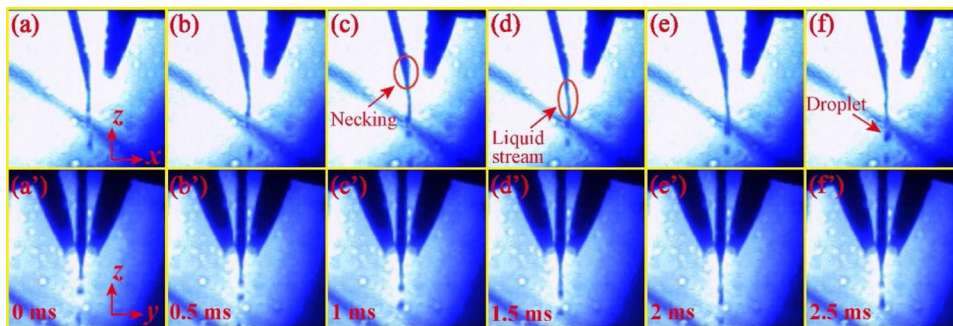
Fig. 5 The droplet transfer process of T-TIG-MIG indirect arc welding with a current of 120 A + 120 A under a WFS of 295 cm/min: **a**, **a'** 0 ms; **b**, **b'** 1.5 ms; **c**, **c'** 3 ms; **d**, **d'** 4.5 ms; **e**, **e'** 6 ms; **f**, **f'** 8.5 ms

Fig. 6 The droplet transfer process of T-TIG-MIG indirect arc welding with a current of 120 A + 120 A under a WFS of 335 cm/min: **a**, **a'** 0 ms; **b**, b' 0.5 ms; **c**, **c'** 1 ms; **d**, **d'** 1.5 ms; **e**, **e'** 2 ms; **f**, **f'** 2.5 ms

Fig. 7 The droplet transfer process of T-TIG-MIG indirect arc welding with a current of 120 A + 120 A under a WFS of 375 cm/min: **a**, **a'** 0 ms; **b**, **b'** 1.5 ms; **c**, **c'** 3 ms; **d**, **d'** 4.5 ms; **e**, **e'** 5 ms; **f**, **f'** 5.5 ms
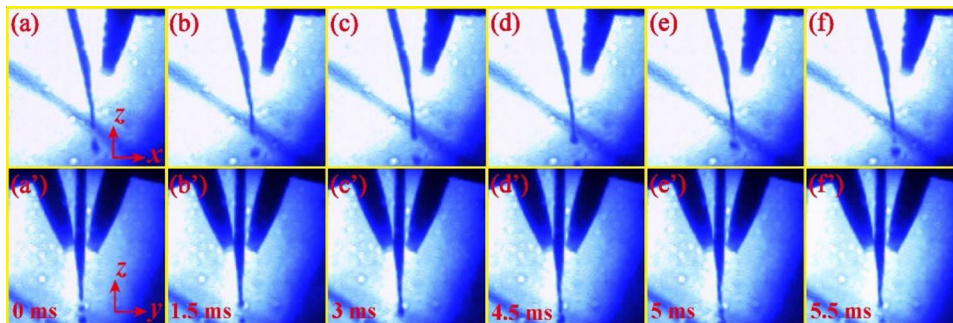
lower left of the tungsten tips in the *xOz* plane, and the liquid metal accumulated to form a fluid beam. The droplet transfer mode still belonged to streaming spray transfer. However, the diameter and length of the liquid stream increased a little, and the time of droplet growth slightly increased again. Besides, the droplet trajectory shifted to the electrode side in the *xOz* plane without deflection in the *yOz* plane.

Figure 8 shows the distributions of the droplet size and transfer frequency under different WFSs. As the WFS increased, the droplet diameter firstly decreased and subsequently increased, while the change of the transfer frequency was the opposite. The droplet transfer mode changed from projected spray transfer to streaming spray transfer accordingly. Moreover, it could be seen that when the WFS was in the range of 315–340 cm/min, the melting speed of the wire was relatively higher, and the droplet was detached from the wire more smoothly. Therefore, the WFSs in this range could be regarded as the optimized values for T-TIG-MIG indirect arc welding with a current of 120 A + 120 A in this experiment. In addition, combined with the droplet transfer process in Fig. 6, it could be inferred that the vicinity of the tungsten tips was an ideal position only from the aspect of promoting the droplet detachment.

Arc current, arc voltage, and the interaction of the above two significantly influenced the characteristics of droplet transfer [16]. Figures 9, 10, and 11 show the droplet transfer processes of T-TIG-MIG indirect arc welding under different currents, each of which was matched with the optimized WFS. It could be seen that different currents also resulted in different droplet transfer processes.

When the current was small, as shown in Fig. 9, the melting speed of the wire was extremely low due to the small thermal power, and the molten metal formed a big ball droplet under the surface tension; hence, the time of droplet growth was considerably long. The droplet transfer mode belonged to globular transfer [17]. The diameter of the droplet was significantly larger than that of the wire, and the transfer frequency was as low as 4 Hz. In addition, the end of the wire had a significant fluctuation, which affected the arc length and arc stability.
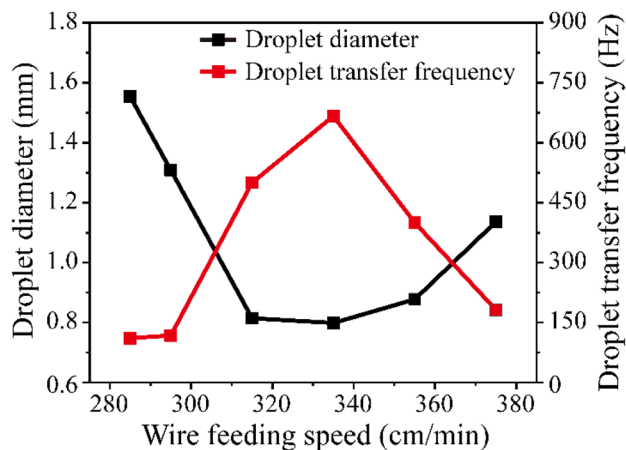

Fig. 8 The distributions of the droplet diameter and transfer frequency of T-TIG-MIG indirect arc welding with a current of 120 A + 120 A under different WFSs
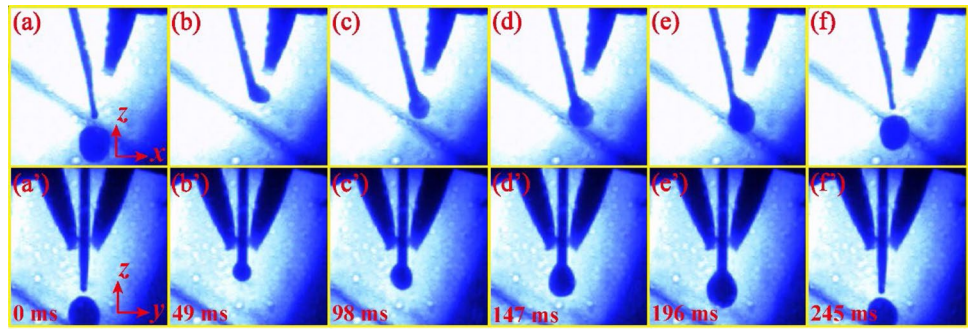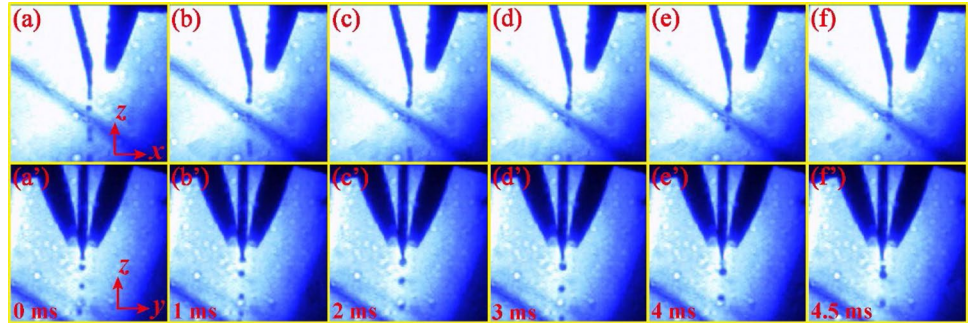
Fig. 9 The droplet transfer process of T-TIG-MIG indirect arc welding with a current of 60 A + 60 A under a WFS of 160 cm/min: **a**, **a'** 0 ms; **b**, **b'** 49 ms; **c**, **c'** 98 ms; **d**, **d'** 147 ms; **e**, **e'** 196 ms; **f**, **f'** 245 ms
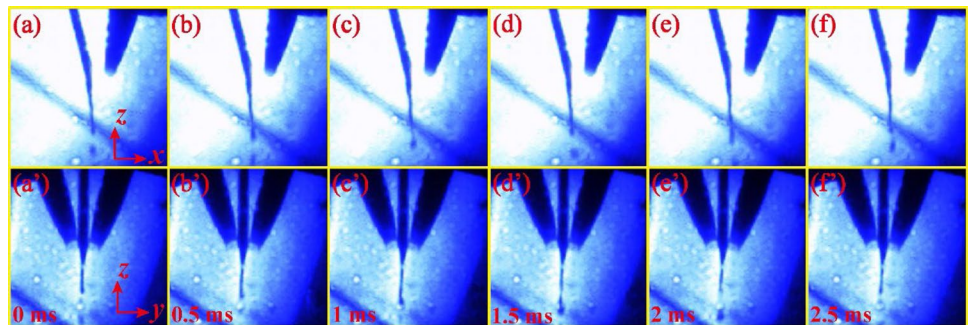
Fig. 10 The droplet transfer process of T-TIG-MIG indirect arc welding with a current of 100 A + 100 A under a WFS of 250 cm/min: **a**, **a'** 0 ms; **b**, **b'** 1 ms; **c**, **c'** 2 ms; **d**, **d'** 3 ms; **e**, **e'** 4 ms; **f**, **f'** 4.5 ms

Fig. 11 The droplet transfer process of T-TIG-MIG indirect arc welding with a current of 140 A + 140 A under a WFS of 410 cm/min: **a**, **a'** 0 ms; **b**, **b'** 0.5 ms; **c**, **c'** 1 ms; **d**, **d'** 1.5 ms; **e**, **e'** 2 ms; **f**, **f'** 2.5 ms

As shown in Figs. 10 and 11, when the current increased to a higher level, the wire end had a necking phenomenon, and a liquid stream was formed below the wire. The droplet transfer mode changed into a streaming spray transfer. The diameter of the droplet decreased significantly, and the transfer frequency increased considerably. Additionally, the position of the wire end was stable with only a slight fluctuation, which was beneficial to the arc conduction structure. Furthermore, with the further increase of the current, the length of the liquid stream increased accordingly.

Figure 12 shows the distributions of the droplet diameter and transfer frequency under different welding currents. With the increase of the welding current, the diameter of the droplet gradually decreased, while the transfer frequency gradually increased. The droplet transfer mode changed from the globular transfer to the streaming spray transfer accordingly. What is more, the diameter of the droplet dramatically
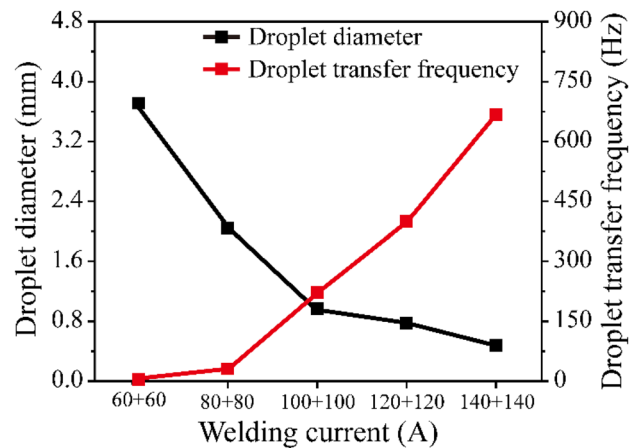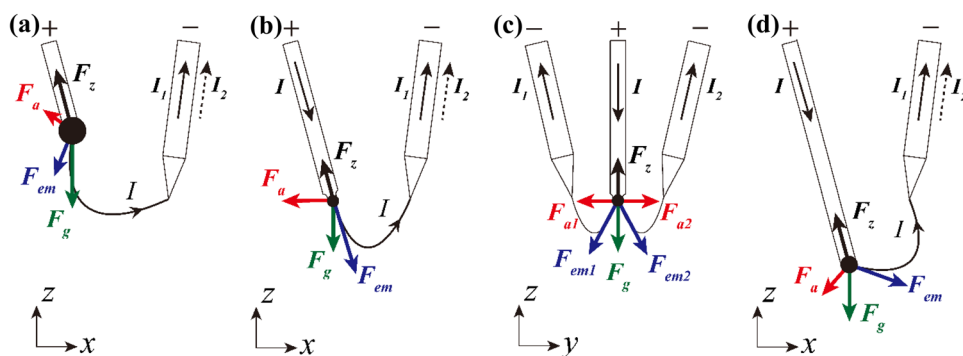
Fig. 12 The distributions of the droplet diameter and transfer frequency of T-TIG-MIG indirect arc welding with different currents under the corresponding WFSs

Fig. 13 Force analysis on the droplet in T-TIG-MIG indirect arc welding: **a** low WFS; **b**, **c** optimized WFS; and **d** high WFS

decreased to a value less than the wire diameter when the current was about 100 A + 100 A. Consequently, combined with the droplet transfer process in Fig. 10, it could be roughly inferred that the critical current that the streaming spray transfer occurred was almost 100 A + 100 A in this experiment.

The droplet transfer behavior was directly determined by arc heat and the forces acting on it, which varied with the welding condition. The dynamic-force balance theory [18] would be adopted to conduct preliminary force analysis for T-TIG-MIG indirect arc welding. In conventional GMAW, the major forces acting on the droplet included gravity, electromagnetic force, surface tension, aerodynamic drag force, and momentum force [19]. Among them, the aerodynamic drag force and momentum force were relatively small compared to other forces, according to the approximate calculation and estimation in the reference [20]. Therefore, they would be neglected in the following analysis in this study.

Different from conventional GMAW, the arc pressure F_a was an additional force acting on the droplet in T-TIG-MIG indirect arc welding because of the special conductive structure established between the wire and the electrodes.

Figure 13 shows the force analysis on the droplet in T-TIG-MIG indirect arc welding. When the WFS was small in Fig. 13a, the current density and the arc temperature were low due to the dispersed arc. On the one hand, the electromagnetic force F_{em}, a primary one of detaching forces, was low; on the other hand, the surface tension F_σ, one primary sustaining force, was high, because the surface tension coefficient was inversely proportional to the temperature. Besides, in Fig. 13a, the component of the arc pressure F_a on the wire axis pointed upward, and thus prevented the droplet from detaching. Therefore, the droplet was detached not smoothly with a large diameter and small transfer frequency. When the WFS was optimized, the wire end was located in the vicinity of the tungsten tips in Fig. 13b, c, the droplet could absorb more heat from the concentrated arc, and thus the surface tension F_σ decreased accordingly. Besides, the electromagnetic force F_{em} and the arc pressure F_a increased significantly, since the arc pressure presented a positive relationship with the

current density [21]. As a result, the detaching forces were considerably larger than the sustaining forces, which made the droplet transfer process dramatically smooth in Fig. 6. In addition, the electromagnetic forces F_{em1} and F_{em2}, as well as the arc pressure F_{a1} and F_{a2}, were symmetrical in the yOz plane, which was beneficial to regulate the droplet trajectory. However, when WFS was relatively large in Fig. 13d, the detaching forces slightly decreased again due to the elongated arc, which would impede the droplet transfer to a certain extent.

When the welding current was smaller than the critical value, the electromagnetic force F_{em} and the arc pressure F_a were significantly low. Meanwhile, the arc temperature was considerably low so that the surface tension F_σ was substantially high. Therefore, the droplet was extremely difficult to detach from the wire end. Eventually, the droplet would grow to a larger size to achieve a larger gravity F_g to overcome the surface tension and thus presented a large globular transfer process in Fig. 9. However, when the welding current increased and exceeded the critical
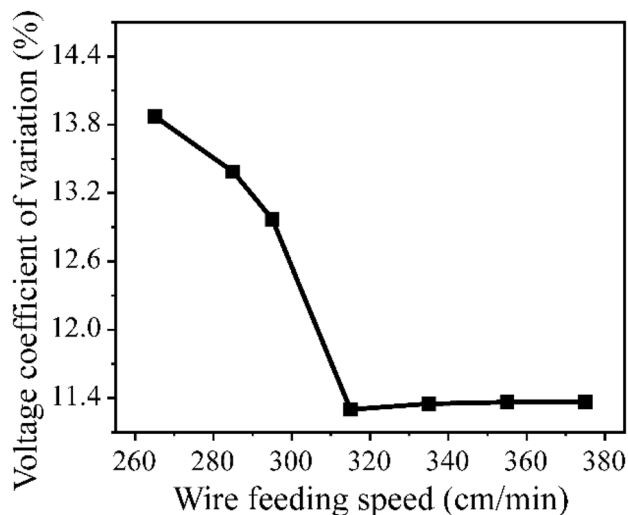

Fig. 14 The distribution of the arc voltage coefficient of variation of T-TIG-MIG indirect arc welding with a current of 120 A + 120 A under different WFSs

value, the detaching forces increased considerably, while the sustaining forces decreased substantially. Therefore, the droplet transfer process became dramatically smooth and finally showed streaming spray transfer in Figs. 10 and 11.

3.3 Stability analysis

In this experiment, T-TIG-MIG indirect arc welding was powered by constant current mode; thus, the fluctuation of the arc voltage could directly reflect the stability of the welding process. The fluctuation could be quantitatively analyzed by the voltage coefficient of variation η according to statistical methods,

$$\eta = \sqrt{[\sum_{i=1}^{n} (U_i - \overline{U})^2 \overline{U}/(n-1)]} \times 100\% \tag{1}$$

where η is the voltage coefficient of variation, $\overline{U}$ is the average voltage, and U_i is the voltage of the i-th sample. The smaller the η was, the more stable the welding process became.

Figure 14 shows the distribution of the voltage coefficient of variation of T-TIG-MIG indirect arc welding with a current of 120 A + 120 A under different WFSs. As the WFS increased, the η firstly decreased steeply and then increased slightly. What is more, when the WFS reached 315 cm/min, the η reached the minimum value. In addition, combining with the arc shape and droplet transfer behavior in Figs. 2 and 6, when the η was relatively low, the position of the droplet detachment from the wire was in the vicinity of the tungsten tips. This was closely related to the fact that the arc was more concentrated with higher stiffness, and the droplet was detached more smoothly with a smaller size and lower transfer period. However, the η was significantly high when the WFS was relatively small, which might be caused by the significant fluctuation of the arc length and the irregular droplet trajectory.

Figure 15 shows the distribution of the voltage coefficient of variation of T-TIG-MIG indirect arc welding with different currents. It could be seen that with the increase of welding current, the η gradually decreased, which meant that the increase of the welding current was beneficial to the process stability. When the current was relatively low, the droplet diameter was considerably large, which caused that every time the droplet was separated from the wire, the arc length, and the contact area between the terminal of the wire, and the arc changed sharply. However, when the current exceeded the critical current, the droplet transfer mode changed into streaming spray transfer, and a stable transfer process was achieved. Moreover, the greater current density
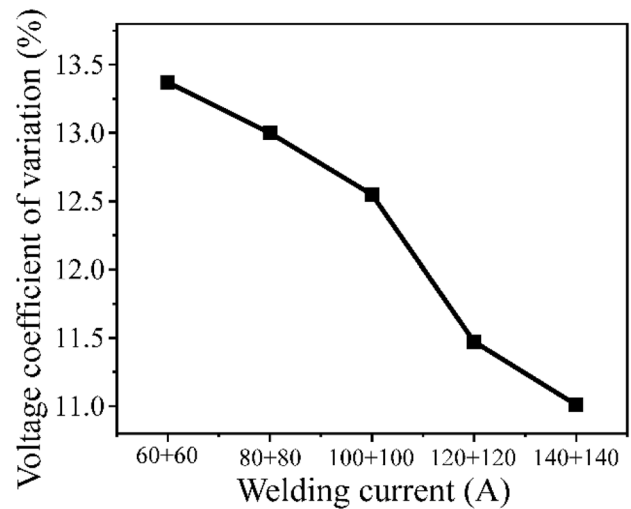
Fig. 15 The distribution of the arc voltage coefficient of variation of T-TIG-MIG indirect arc welding with different currents under the corresponding WFSs

and higher arc stiffness due to the higher welding current were also beneficial to the arc stability. For all these above experiment phenomena, as long as using suitable welding parameters, one-wire and two-electrode configurations could also achieve a stable arc shape and metal transfer process.

3.4 Weld bead

The weld bead formations and cross-sectional shapes of T-TIG-MIG indirect arc welding under different currents with optimized WFSs are shown in Fig. 16a−c. It could be seen that the weld beads were continuous and smooth. As the welding current increased, the ratio of weld reinforcement to weld width decreased gradually, and the wetting angle increased gradually. In other words, the increase in welding current promoted the spreadability of the weld bead. Due to the increase of the welding current, the temperature of the arc and the heat carried by the droplet increased accordingly, and arc length also increased. Therefore, the heat input to the workpiece increased accordingly, which was beneficial to the fluidity of the molten metal on the workpiece.

Figure 16d shows the weld bead appearance and cross-sectional shape of the conventional cold-wire T-TIG welding process under 120 A + 120 A current with the WFS of 110 cm/min. This WFS was also the maximum value that could achieve weld formation under this experimental condition. It could be seen that the weld bead became uneven with a large range of the heat-affected zone (HAZ). From Fig. 16c′, d′, compared to conventional cold-wire T-TIG welding process under the same current, the wire deposition rate of T-TIG-MIG indirect arc was increased by about 186% times, while the range

Fig. 16 The weld formations and the cross sections of T-TIG-MIG indirect arc welding: **a**, **a′** 80 A + 80 A, 200 cm/min; **b**, **b′** 100 A + 100 A, 250 cm/min; **c**, **c′** 120 A + 120 A, 315 cm/min, and of **d**, **d′** conventional cold-wire T-TIG welding with a current of 120 A + 120 A under the WFS of 110 cm/min
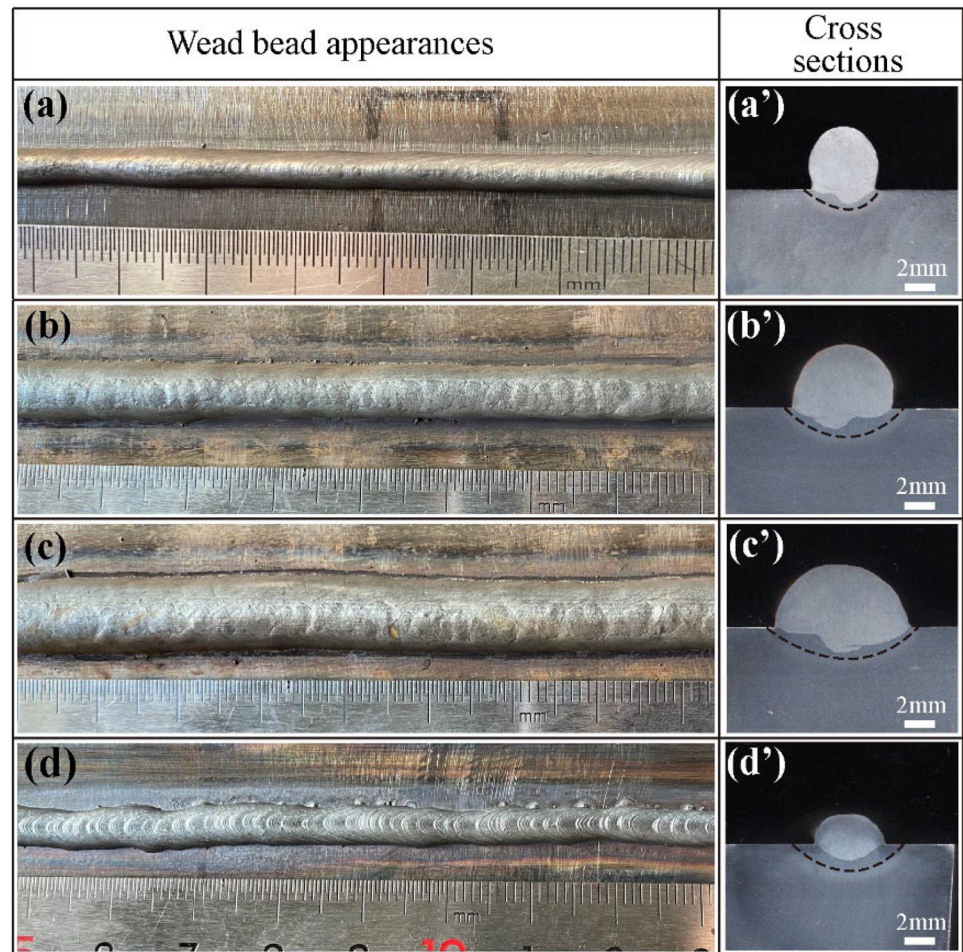
of the HAZ was reduced by about 41%. Compared to the conventional cold-wire T-TIG welding process, on the one hand, the wire-melting mechanism of the T-TIG-MIG indirect arc was significantly different, in which the wire melting mainly relied on the heat production in the anode zone of the arc, instead of the weld pool, so the melting efficiency of the wire was improved considerably; on the other hand, the workpiece was not in the arc current loop, and thus the heat input to the workpiece mainly consisted of the convection heat of the arc column and heat carried by droplet, which was much smaller. Therefore, the T-TIG-MIG indirect arc could not only achieve a stable welding process but also considerably improve wire deposition rate and reduce heat input to the workpiece.

4 Conclusions

The paper proposed a T-TIG-MIG indirect arc welding method and mainly investigated arc behavior and the droplet transfer process. The specific conclusions were as follows:

1. T-TIG-MIG indirect arc burnt between a wire and two tungsten electrodes and was essentially formed by the coupling of two single-electrode TIG-MIG indirect arcs. The arc shape was mainly determined by the electromagnetic force and the plasma jet force acting on the charged particles in the upper arc column. Besides, different from conventional GMAW, the arc pressure was a crucial additional force acting on the droplet.

2. For a certain welding current, there existed an optimized range of wire feeding speed, where the arc was more concentrated with a higher coupling degree. With the increase of the welding current, the arc length and stiffness increased gradually. Especially, when the current exceeded the critical current, the electromagnetic forces and arc pressure acting on the droplet were significantly larger than the sustaining forces; therefore, it showed streaming spray transfer, and thus superior process stability.

3. In T-TIG-MIG indirect arc welding, the wire melting mainly relied on the heat production in the anode zone of the arc, while the heat input to the workpiece mainly consisted of the convection heat of the arc column and

heat carried by droplet. Therefore, under the same current, the wire deposition rate of T-TIG-MIG indirect arc welding increased by about 186% times, while the range of the heat-affected zone was reduced by about 41%.

Declarations

References

1. Zhang Y, Yang Y, Zhang W, Na S (2020) Advanced welding manufacturing: a brief analysis and review of challenges and solutions. J Manuf Sci Eng Trans ASME 142:110816

2. Wang Z, Jiang D, Wu J, Xu M (2020) A review on high-frequency pulsed arc welding. J Manuf Process 60:503–519

3. Zou S, Wang Z, Hu S, Zhao G, Wang W, Chen Y (2020) Effects of filler wire intervention on gas tungsten arc: Part I - mechanism. Weld J 99:246s–254s

4. Ungethüm T, Spaniol E, Hertel M, Füssel U (2020) Analysis of metal transfer and weld geometry in hot-wire GTAW with indirect resistive heating. Weld World 64:2109–2117

5. Lv S, Tian X, Wang H, Yang S (2007) Arc heating hot wire assisted arc welding technique for low resistance welding wire. Sci Technol Weld Join 12:431–435

6. Voigt AL, Cunha TV, Niño CE (2020) Conception, implementation and evaluation of induction wire heating system applied to hot wire GTAW (IHW-GTAW). J Mater Process Technol 281:116615

7. Chen J, Lu Y, Li X, Zhang Y (2012) Gas tungsten arc welding using an arcing wire. Weld J 91:261s–269s

8. Wang J, Wu D, Liao P, Tian C, Li M, Feng J (2013) Metal transfer and arc behaviour of novel consumable and non-consumable electrode indirect arc droplet welding. Sci Technol Weld Join 18:261–270

9. Kobayashi K, Yamada M, Fujishima K, Iijima T, Ushio M (2004) Development of high efficiency twin-arc TIG welding method. IIW Doc XII: 1669–1701

10. Leng X, Zhang G, Wu L (2006) The characteristic of twin-electrode TIG coupling arc pressure. J Phys D Appl Phys 39:1120–1126

11. Leng X, Zhang G, Wu L (2006) Experimental study on improving welding efficiency of twin electrode TIG welding method. Sci Technol Weld Join 11:550–554

12. Chen S, Wang L, Xiao J, Wei P (2018) Arc behavior and droplet dynamics of AC GTAW-GMAW hybrid indirect arc. Weld J 97:91–98

13. Ando K, Hasegawa M (1985) The phenomenon of welding arc. China Machine Press, Beijing

14. Yang M, Yang Z, Qi B (2015) The effect of pulsed frequency on the plasma jet force with ultra high-frequency pulsed arc welding. Weld World 59:875–882

15. Lu Y, Chen S, Shi Y, Li X, Chen J, Kvidahl L, Zhang Y (2014) Double-electrode arc welding process: principle, variants, control and developments. J Manuf Process 16:93–108

16. Zhao Y, Chung H (2018) Numerical simulation of the transition of metal transfer from globular to spray mode in gas metal arc welding using phase field method. J Mater Process Technol 251:251–261

17. Huang J, Pan W, Yang W, Xue C, Shi Y, Fan D (2019) The influence of bypass current on metal transfer in dual-bypass gas metal arc welding. J Manuf Process 38:179–186

18. Choi JH, Lee J, Yoo CD (2001) Dynamic force balance model for metal transfer analysis in arc welding. J Phys D Appl Phys 34:2658–2664

19. Kim YS, Eager TW (1993) Analysis of metal transfer in gas metal arc welding. Weld J 72:269s–278s

20. Huang Y, Shao Y, Zhang Y (2012) Nonlinear modeling of dynamic metal transfer in laser-enhanced GMAW. Weld J 91:140s–148s

21. Lin ML, Eagar TW (1986) Pressures produced by gas tungsten arcs. Metall Trans B 17:601–607